PHYSICAL REVIEW B VOLUME 32, NUMBER 4 15 AUGUST 1985

Curved-wave-front corrections for photoelectron scattering

J. J. Barton and D. A. Shirley
Materials and Molecular Research Division, Lawrence Berkeley Laboratory, University of California, Berkeley, California 94720
and Department of Chemistry, University of California, Berkeley, California 94720
(Received 1 April 1985)

We derive new, simplified formulas for the scattering of $l=1$ spherical waves from central potentials, as a basis for discussing curved-wave-front corrections to single-scattering plane-wave models for angle-resolved photoemission extended fine structure and extended x-ray-absorption fine structure. A differential form for the expansion of the screened spherical wave replaces the usual Gaunt-integral form to facilitate the summation over equivalent magnetic sublevels in the scattered wave. Spherical-wave scattering factors are defined and interpreted as corrections to the plane-wave scattering factor. We argue and demonstrate by example that the remarkable success of plane-wave models does not result from reaching the spherical-wave asymptotic limit; instead, successive partial-wave corrections cancel for backscattering at high energy. The new scattering formulas allow curved-wave-front numerical calculations to be performed with little more effort than with plane-wave formulas.

I. INTRODUCTION

Understanding the motion of unbound electrons in solids is an interesting problem with important implications for surface structure determination methods based on electron scattering. The energy range from 20 to 200 eV has been studied extensively as a basis for the analysis of low-energy electron diffraction (LEED) data;[1–3] more recent work in the energy range 50—1000 eV has been inspired by the explosive growth in the number of extended x-ray-absorption fine structure (EXAFS) measurements.[4] In the case of LEED, the incident electron plane wave is simply described, but it excites every atom in the surface region, leading to a complex scattering problem; in the case of EXAFS only a single chemical element is excited by the x-ray beam, but the entire x-ray absorption process must be understood and the observed modulations correspond to a special multiple-scattering event.[5] Thus we suggest that an even more recent technique,[6] angle-resolved photoemission extended fine structure (ARPEFS), may be a more straightforward measurement for further understanding of electron scattering in the 50—1000-eV range. ARPEFS measures partial cross-section oscillations of photoelectrons: only electrons from a single chemical element are measured and a 4π angular integration is not necessary. This paper investigates one aspect of the theory of electron scattering in solids, the role of curved-wave corrections to the plane-wave single-scattering of $(1s)$ photoelectrons.

A more practical motivation for this work is the interesting discrepancy between ARPEFS measurements and simple scattering theory results for the $c(2\times2)$S/Ni(100) system. Experimentally, a relatively simple Fourier transform spectrum led to the conclusion that only nearest-neighbor and backscattering nonneighboring atoms contributed substantially to the observed spectrum.[6] In other words, the number of important scattering atoms was small, permitting a simple interpretation of the Fourier spectrum. This conclusion has been recently challenged by Bullock, Fadley, and Orders[7] on the basis of single-scattering, plane-wave theoretical calculations. They demonstrated that a great many ion cores should contribute to the theoretical curve under these and certain other approximations and hence no simple assignment of the Fourier peaks should be possible. Unfortunately, the reproduction of the experimental oscillations by these theoretical calculations is very poor, and we are led to question the conclusions drawn from them.

To settle this issue, an improved theoretical calculation capable of matching the measured curves within experimental accuracy seems in order; if we know that the sum of the calculated scattering events is correct, then we can compare the relative intensity of these events with more confidence. The plane-wave single-scattering calculations may be improved by the following:

(i) a more accurate atomiclike photoemission wave function (unscattered, direct wave);
(ii) curved-wave corrections;
(iii) multiple scattering;
(iv) improved elastic scattering phase shifts; and
(v) more accurate inelastic damping.

These improvements are somewhat entwined, but in this paper we will concentrate on a single issue: When are curved-wave (also called spherical-wave) corrections important?

We will examine only the simplest case of spherical-wave scattering: single scattering of photoelectrons excited from a $(1s)$ core level. We derive new formulas for this scattering in Sec. II, applicable to both ARPEFS and EXAFS experiments. These formulas facilitate a qualitative discussion of curved-wave corrections which is presented in Sec. III. In Sec. IV we evaluate individual terms in these formulas for the example of a Ni atom potential. Our discussion in Sec. V centers on possible gen-

eralizations to higher angular momenta. Finally, we address the impact our results might have on calculation of extended fine structure.

II. CURVED-WAVE SCATTERING OF $l=1$ PHOTOELECTRONS

Our scattering system consists of a photoemitting atom and an array of nonoverlapping ion-core potentials. Zeroth-order calculation of the photoemission partial cross section would ignore the ion core array and only consider the atomiclike photoabsorption. Corrections caused by scattering from the ion-core potentials gives the ARPEFS oscillations. Since we are only concerned with the oscillations, the details of zeroth-order calculation are not relevant: we need only know the zeroth-order wave function. With dipole selection rules, polarized light, a $(1s)$ core-level initial state, and complete metallic screening the zeroth-order wave function is proportional to

$$\psi_0(\mathbf{r})=ih_1(kr)Y_{10}(\hat{\mathbf{r}}) . \tag{1}$$

Here $h_l(kr)$ is the spherical Hankel function of the first kind[8] [we will omit the usual superscript (1) as in $h_l^{(1)}(kr)$ and we will not use spherical Hankel functions of the second kind], $Y_{lm}(\hat{\mathbf{r}})$ is the spherical harmonic evaluated at the angles given by the unit vector $\hat{\mathbf{r}}$ in the direction of $\mathbf{r}$, and k is the electron's wave number far from the photoemitter. Notice that we have selected the polarization vector of the light for our $\hat{\mathbf{z}}$ axis to simplify the zeroth-order wave-function description. The first-order corrections to this wave function are generated by including scattered waves emanating from each nearby ion core. The partial-wave method[9] for calculating these scattered waves has three steps:

(i) expand the incident wave as an angular momentum series about the ion-core position;

(ii) multiply each partial wave in this series by a (complex) scattering amplitude (which also shifts the wave phase);

(iii) sum the nonzero partial waves to give the full scattered wave.

It is the first step which distinguishes plane-wave from spherical-wave scattering.

A. Plane waves

As a basis for our discussion of the curved-wave effects we repeat the derivation of the plane-wave ARPEFS model first presented by Lee,[5] but following more closely the method used by Lee and Pendry[10] in their derivation of the EXAFS formula.

In a plane-wave approximation,[5] the photoelectron wave is represented near the scattering center by the value of the wave at the center, times a plane wave:

$$\psi_0(\mathbf{r})\approx ih_1(ka)\left[\frac{3}{4\pi}\right]^{1/2}(\cos\theta_{\varepsilon\mathbf{a}})e^{ik\hat{\mathbf{a}}\cdot(\mathbf{r}-\mathbf{a})} , \tag{2}$$

where $\theta_{\varepsilon\mathbf{a}}$ is the angle between the electric vector $\hat{\boldsymbol{\varepsilon}}$ and the bond vector $\mathbf{a}$. Since we have already ignored wave-front curvature with this approximation, we replace the Hankel function by its asymptotic limit,

$$i^l h_l(ka)\sim\frac{e^{ika}}{ika} \tag{3}$$

and apply the well known Bauer formula,

$$e^{i\mathbf{k}\cdot\mathbf{r}}=\sum_{l=0}^{\infty}(2l+1)i^l j_l(kr)P_l(\cos\theta_{\mathbf{kr}}) , \tag{4}$$

to expand the photoelectron wave around the scattering center:

$$\psi_0(\mathbf{r})\approx\left[\frac{3}{4\pi}\right]^{1/2}\cos\theta_{\varepsilon\mathbf{a}}\frac{e^{ika}}{ika}\sum_{l=0}^{\infty}(2l+1)i^l j_l(kr')\times P_l(\cos\theta_{\mathbf{ar}'}) . \tag{5}$$

Here $j_l(kr)$ is the incoming spherical Bessel function, $P_l(\cos\theta)$ is the Legendre polynomial, and $\mathbf{r}'=\mathbf{r}-\mathbf{a}$. The scattering angle, $\theta_{\mathbf{ar}'}$, is defined as the angle between the propagation vector for the incident plane wave, $k\hat{\mathbf{a}}$, and the outgoing wave direction $\mathbf{r}'$.

To construct the scattered wave, we multiply each incoming partial wave by

$$T_l(k)=\tfrac{1}{2}(e^{2i\delta_l}-1)=i(\sin\delta_l)e^{i\delta_l} , \tag{6}$$

where $\delta_l(k)$ is the partial-wave phase shift. Summing the new outgoing wave gives

$$\psi_{\mathbf{a}}(\mathbf{r}')=\left[\frac{3}{4\pi}\right]^{1/2}\cos\theta_{\varepsilon\mathbf{a}}\frac{e^{ika}}{ika}\times\sum_{l=0}^{l_{\max}}(2l+1)T_l(k)i^l h_l(kr')P_l(\cos\theta_{\mathbf{ar}'}) . \tag{7}$$

The sum of l may be stopped at $l_{\max}$ when all higher partial waves have negligible amplitude, $|T_l(k)|\sim 0$, $l>l_{\max}$. At the angle-resolved detector, located along $\mathbf{R}$, we may replace the outgoing spherical waves by their asymptotic limit. Then a scattering factor is defined by

$$f_{\mathbf{aR}}(k)=\frac{1}{ik}\sum_{l=0}^{l_{\max}}(2l+1)T_l(k)P_l(\cos\theta_{\mathbf{aR}}) \tag{8}$$

to give the scattered wave at the detector as

$$\psi_{\mathbf{a}}(\mathbf{R})=\left[\frac{3}{4\pi}\right]^{1/2}\cos\theta_{\varepsilon\mathbf{a}}\frac{e^{ik|\mathbf{R}-\mathbf{a}|}}{ikR}\frac{e^{ika}}{a}f_{\mathbf{aR}} . \tag{9}$$

The factor $\exp(ik|\mathbf{R}-\mathbf{a}|)$ corrects for the different origin of the scattered wave and for $|\mathbf{R}|\gg|\mathbf{a}|$ we have $|\mathbf{R}-\mathbf{a}|\sim|\mathbf{R}|-|\mathbf{a}|\cos\theta_{\mathbf{aR}}$.

The direct wave at the detector is

$$\psi_0(\mathbf{R})=\left[\frac{3}{4\pi}\right]^{1/2}\cos\theta_{\varepsilon\mathbf{R}}\frac{e^{ikR}}{ikR} , \tag{10}$$

and we calculate the ARPEFS oscillations due to a single atom as

$$\chi(k)=\frac{(\psi_0+\psi_a)^*(\psi_0+\psi_a)}{\psi_0^*\psi_0}-1$$
$$=\frac{2\,|f_{aR}|}{a}\frac{\cos\theta_{\varepsilon a}}{\cos\theta_{\varepsilon R}}\cos[ka(1-\cos\theta_{aR})+\phi_{aR}]\,, \quad (11)$$

where $f_{aR}(k)=|f_{aR}|\exp(i\phi_{aR})$. This formula has been used to analyze experimental ARPEFS data in Ref. 6.

B. Spherical waves

For spherical waves, the angular momentum expansion in its usual form is much more complex:[11]

$$ih_1(kr)Y_{10}(\hat{\mathbf{r}})=\sum_{l'',m''}G_{10l''m''}i^{l''}j_{l''}(kr')Y_{l''m''}(\hat{\mathbf{r}}')\,,$$
$$G_{10l''m''}=\sum_{l',m'}4\pi i^{l'}h_{l'}(ka)Y^*_{l'm'}(\hat{\mathbf{a}})$$
$$\times\int Y_{10}(\hat{\mathbf{k}})Y_{l'm'}(\hat{\mathbf{k}})Y^*_{l''m''}(\hat{\mathbf{k}})d\hat{\mathbf{k}}\,, \quad (12)$$

where $\mathbf{r}'+\mathbf{a}=\mathbf{r}$. This formula is the basis for Lee and Pendry's curved-wave EXAFS formula.[10] To make physical arguments about the nature of curved-wave corrections to the plane-wave formula, we need a simpler form for this expansion, which we will refer to as an origin-shift addition theorem.

An alternative expansion for spherical waves may be derived most readily from Nozawa's original paper[12] which describes expansions of "Helmholt's solid harmonics," his term for the product of spherical Bessel functions and spherical harmonics, which we will call "spherical waves." Nozawa demonstrated that the origin-shift addition theorem results when raising the operator for Helmholtz's solid harmonics,[13]

$$i^l h_l(kr)P_l^m(\cos\theta)e^{im\phi}$$
$$=\left[\frac{-i}{k}\right]^m\left[\frac{\partial}{\partial x}+\frac{i\partial}{\partial y}\right]^m P_l^{(m)}\left[\frac{-i}{k}\frac{\partial}{\partial z}\right]h_0(kr)\,, \quad (13)$$

is applied to the origin-shift addition theorem for $h_0(kr)$:

$$h_0(kr)=\sum_{l=0}^{\infty}(2l+1)i^l j_l(kr')i^l h_l(ka)P_l(\cos\theta_{ar'})\,. \quad (14)$$

Here $P_l^{(m)}(-ik^{-1}\partial/\partial z)$ is the operator obtained by using $(-ik^{-1}\partial/\partial z)$ as the argument of the mth derivative of the Legendre polynomial of order l. As we shall see, this differential form for the expansion eliminates the need for magnetic quantum numbers for the outgoing scattered wave and leaves explicit the angle dependence hidden within $G_{lml''m''}$ above.

For our particular case the raising operator formula is

$$ih_1(kr)P_1(\cos\theta)=\left[-\frac{i}{k}\frac{\partial}{\partial z}\right]h_0(kr) \quad (15)$$

and the origin-shift addition theorem becomes[14]

$$ih_1(kr)P_1(\cos\theta)=\sum_{l''=0}^{\infty}\Bigg[(2l+1)i^{l''}j_{l''}(kr')h_0(ka)$$
$$\times\Bigg[d_1(ka)P_1(\cos\theta_{\varepsilon a})d_{l''}(ka)P_{l''}(\cos\theta_{aR'})-i\cos\theta_{\varepsilon a}\frac{\partial d_{l''(ka)}}{\partial(ka)}P_{l''}(\cos\theta_{ar'})$$
$$-i\,\frac{\cos\theta_{\varepsilon r'}-\cos\theta_{\varepsilon a}\cos\theta_{ar'}}{ka}d_{l''}(ka)\frac{\partial P_{l''}(\cos\theta_{ar'})}{\partial(\cos\theta_{ar'})}\Bigg]\Bigg]\,. \quad (16)$$

We have introduced $d_{l''}(ka)$ to represent the polynomial part of the spherical Hankel function:

$$i^{l''}h_{l''}(ka)=\frac{e^{ika}}{ika}d_{l''}(ka)=h_0(ka)d_{l''}(ka)\,. \quad (17)$$

Note that for large $ka\gg l''(l''+1)$, $d_{l''}(ka)=1.0$, and that $d_l(ka)$ may be calculated by recursion: $d_{l+1}=d_{l-1}-d_l(2l+1)/ika$.

As before, the scattered wave may be calculated by multiplying each incoming partial-wave amplitude by $T_l(k)$ to generate an outgoing partial wave; each outgoing wave may be replaced by its asymptotic limit when the amplitude is calculated at the detector, position $\mathbf{R}$.

We invent a generalized scattering factor based on our origin-shift formula as

$$f_{aR}^{nm}=\frac{1}{ik}\sum_{l''=0}^{l_{\max}}(2l''+1)T_{l''}(k)\frac{\partial^n d_{l''}(ka)}{\partial(ka)^n}\frac{\partial^m P_{l''}(\cos\theta_{aR})}{\partial(\cos\theta_{aR})^m}\,, \quad (18)$$

and the scattered wave is then

$$\psi_a(\mathbf{R})=\left[\frac{3}{4\pi}\right]^{1/2}\frac{e^{ik|\mathbf{R}-\mathbf{a}|}}{ikR}\frac{e^{ika}}{a}$$
$$\times\left[d_1(ka)(\cos\theta_{\varepsilon a})f_{aR}^{00}-i(\cos\theta_{\varepsilon a})f_{aR}^{10}\right.$$
$$\left.-\frac{i}{ka}f_{aR}^{01}(\cos\theta_{\varepsilon R}-\cos\theta_{\varepsilon a}\cos\theta_{aR})\right]\,. \quad (19)$$

If we label the factor within the large parentheses $F_{sph}=|F|\exp(i\phi_{sph})$, we parallel the plane-wave construction of $\chi(k)$ to find

$$\chi(k)=2\frac{|F_{sph}|}{a\cos\theta_{\varepsilon R}}\cos[ka(1-\cos\theta_{aR})+\phi_{sph}]\,. \quad (20)$$

Clearly, F_{sph} determines both the amplitude and phase of the oscillations we will measure. As ka becomes large,

the factors f_{aR}^{10} and $f_{aR}^{01}(ka)$ fall to zero, $d_l(ka)$ becomes 1.0, f_{aR}^{00} tends to f_{aR}, and we have

$$F_{\rm sph} \rightarrow f_{aR}\cos\theta_{\varepsilon a} \ . \tag{21}$$

Thus by studying $F_{\rm sph}$ compared to $f_{aR}\cos\theta_{\varepsilon a}$ we can learn when curved wave corrections will influence the single scattering of photoelectrons.

An alternative derivation for this formula is outlined in Appendix A.

The same method may also be applied to calculation of oscillations in the total absorption cross section, the extended x-ray absorption fine structure (EXAFS). Here the scattered wave must be projected back onto the direct wave at the absorbing atom: the oscillations are an interference at the photoemitter. The derivation for $(1s)$ core levels and polarized light is given in Appendix B. If we call

$$E_{\rm sph}=\frac{1}{ik}\sum_{l''=0}^{l_{\max}}\left\{(2l''+1)T_{l''}(k)(-1)^{l''}\left[\cos^2\theta_{\varepsilon a}\left[d_1(ka)d_{l''}(ka)-i\frac{\partial d_{l''}(ka)}{\partial(ka)}\right]^2-\sin^2\theta_{\varepsilon a}\left[\frac{d_{l''}(ka)}{ka}\right]^2\frac{l(l+1)}{2}\right]\right\}, \tag{22}$$

then we compare $E_{\rm sph}$ to $\cos^2\theta_{\varepsilon a}f_{aR}(\pi)$ to examine curved-wave corrections for EXAFS.

We might proceed directly to numerical applications of these formulas, but the qualitative success of the plane-wave approximation suggests that some insight into electron scattering may be gained by examining the individual terms in these spherical-wave formulas compared to results from a plane-wave model. We take up this topic in the next section.

III. NATURE OF THE CURVED-WAVE CORRECTIONS

In this section we examine the formulas derived in the preceding section for the exact single scattering of $l=1$ spherical waves. We know that the plane-wave scattering model is substantially correct so we concentrate on differences caused by allowing for wave-front curvature. We begin this section with a brief examination of the mathematical reduction of the spherical-wave formulas to their plane-wave limit. This provides one method for studying curved-wave effects, but to be more specific we might inquire about the importance of the fundamental spherical nature of the waves which is independent of angular momentum—embodied in $\exp(ikr)/ikr$—compared to additional curved-wave corrections due to the particular incident angular momentum. We will demonstrate that each term in the differential form, Eq. (19), corresponds to specific curved-wave corrections. The first term gives the *basic* correction common to all angular momenta, the second term corrects for additional *radial* structure specific to the incident angular momentum, while the third term corresponds to additional *angular* character specific to angular momentum.

Our curved-wave formulas approach the plane-wave results whenever the spherical Hankel functions can be replaced by their asymptotic limits [Eq. (3)]. In our notation this is equivalent to replacing the polynomial part of the spherical Hankel function, $d_l(ka)$ by 1.0 in our formulas:

$$d_l(ka)=\left[1-\frac{l(l+1)}{2ika}+\cdots\right]\sim 1.0 \ . \tag{23}$$

Thus we must first discuss the size of $l(l+1)/(2ika)$. Notice that the angular momentum in this formula is the scattered-wave angular momentum, not the dipole selection rule momentum from the photoabsorption.

The contribution of each partial wave to the final scattered wave is dictated by the partial-wave amplitude [Eq. (6)]. For every wave number, k, there will be some angular momentum $l_{\max}$ beyond which all partial-wave amplitudes may be neglected. With some criterion for this cutoff we can define an equivalent range, r_0, for the scattering potential:[15]

$$l_{\max}(l_{\max}+1)\sim(kr_0)^2 \ . \tag{24}$$

In other words, the largest significant partial wave climbs in proportion to k. The asymptotic criterion then reads

$$\frac{kr_0}{2}\left[\frac{r_0}{a}\right]\ll 1 \tag{25}$$

for the last significant partial wave. By this analysis we conclude that the spherical Hankel function can be replaced by its limit only for large $a\gg r_0$; higher energy actually leads us away from the limit. Of course, as the number of partial waves increases, the impact of the largest angular momentum on the value of the scattering factor decreases. To properly assess this effect we should consider in detail the weight of each partial wave, but for a crude estimate assume equal weights. Then the contribution of the largest angular momentum decreases roughly like $(1/l_{\max})$, giving an asymptotic criterion for the sum as

$$\frac{1}{2}\left[\frac{r_0}{a}\right]\ll 1 \ . \tag{26}$$

We expect r_0 to be ≈ 1 Å and for $|\mathbf{a}|$ equal to the nearest-neighbor distance, $r_0/2a=0.2$. Under these assumptions the curved-wave effects are not too small; we turn to study the curved-wave formulas for ARPEFS and EXAFS.

For photoelectric scattering we have

$$F_{\rm sph}=d_1(ka)(\cos\theta_{\varepsilon a})f_{aR}^{00}-i(\cos\theta_{\varepsilon a})f_{aR}^{10}-if_{aR}^{01}\left[\frac{\cos\theta_{\varepsilon R}-\cos\theta_{\varepsilon a}\cos\theta_{aR}}{ka}\right] . \tag{27}$$

The first term,

$$d_1(ka)(\cos\theta_{\varepsilon a})f_{aR}^{00}=\left[1+\frac{i}{ka}\right]\frac{\cos\theta_{\varepsilon a}}{ik}\times\sum_{l=0}^{l_{max}}(2l+1)T_l(k)d_l(ka)P_l(\cos\theta_{aR}) \tag{28}$$

is the only one which survives in the asymptotic limit, $ka\gg l(l+1)$. By examining the origin-shift addition theorem for $h_0(kr)$ [Eq. (14)] we can show that this first term corresponds to the single scattering of an $l=0$ wave (the f_{aR}^{00} factor) multiplied by the $l=1$ wave components [the $d_l(ka)\cos\theta_{\varepsilon a}$ part]. The scattering factor f_{aR}^{00} differs from the plane-wave counterpart f_{aR} only by including a weighting on partial waves, $d_l(ka)$, dependent on ka. Since

$$h_0(ka)=\exp(ika)/ika\ ,$$

we can see that this weighting corrects the plane-wave scattering factor for the variation in the spherical wave over the finite size of the ion-core potential due to $(1/ika)$.

The second term,

$$-i(\cos\theta_{\varepsilon a})f_{aR}^{10}=\frac{-i\cos\theta_{\varepsilon a}}{ik}\times\sum_{l=0}^{l_{max}}(2l+1)T_l(k)\frac{\partial d_l(ka)}{\partial(ka)}\times P_l(\cos\theta_{aR})\ , \tag{29}$$

contains the derivative of the polynomial part of the spherical Hankel function. The expansion of d_l in Eq. (23) gives the leading term in the derivative as

$$\frac{\partial d_l(ka)}{\partial(ka)}\sim\frac{1}{ika}\frac{l(l+1)}{2ika}\ . \tag{30}$$

Since $ka\sim 10$ in the ARPEFS energy range we can anticipate this spherical-wave correction being much smaller than the difference between f_{aR}^{00} and f_{aR}: the factor $l(l+1)/2ika$ represents the leading correction to the plane wave form and f_{aR} is smaller by $1/ka$. This term is literally the radial variation of f_{aR}^{00}: It corrects the s-wave origin shift, given by f_{aR}^{00}, for the variation in $h_1(ka)$ over the potential not already contained in f_{aR}^{00}.

The third term,

$$\frac{-i}{ka}(\cos\theta_{\varepsilon R}-\cos\theta_{\varepsilon a}\cos\theta_{aR})f_{aR}^{01}=-i\frac{(\cos\theta_{\varepsilon R}-\cos\theta_{\varepsilon a}\cos\theta_{aR})}{(ka)(ik)}\sum_{l=0}^{l_{max}}(2l+1)T_l(k)d_l(ka)\frac{\partial P_l(\cos\theta_{aR})}{\partial(\cos\theta_{aR})}\ , \tag{31}$$

contains both an unusual angular factor and a derivative with respect to $\cos\theta_{aR}$. This term accounts for the variation in the spherical-wave amplitude laterally across the width of the potential. We can use spherical trigonometry to rewrite this term in an instructive fashion. If we place three unit vectors in the directions of $\hat{\boldsymbol{\varepsilon}}$, the polarization vector **R**, the emission vector, and **a**, the bond vector, at a common origin, then the vector tips will define a spherical triangle on a unit sphere with sides $\theta_{\varepsilon R}$, $\theta_{\varepsilon a}$, and θ_{aR}. Observing this triangle along the vector **a** we see that

$$\cos\theta_{\varepsilon R}-\cos\theta_{\varepsilon a}\cos\theta_{aR}=\sin\theta_{\varepsilon a}\sin\theta_{aR}\cos\phi_{\varepsilon aR}\ , \tag{32}$$

where $\phi_{\varepsilon aR}$ is the dihedral angle between $\boldsymbol{\varepsilon}$ and **R** through **a**. Since the associated Legendre polynomials are defined

$$P_l^m(\cos\theta)=\sin^m\theta\frac{d^mP_l(\cos\theta)}{d(\cos\theta)^m}\ ,\quad 0\le m\le l\ , \tag{33}$$

we can write

$$-i\frac{(\cos\theta_{\varepsilon R}-\cos\theta_{\varepsilon a}\cos\theta_{aR})}{ka}f_{aR}^{01}=\frac{\sin\theta_{\varepsilon a}\cos\theta_{\varepsilon aR}}{ik}\sum_{l=0}^{l_{max}}(2l+1)T_l(k)d_l(ka)\frac{P_l^1(\cos\theta_{aR})}{ika}\ . \tag{34}$$

Thus this correction to the plane-wave form reaches its maximum when the scattering potential is located in the nodal plane ($\cos\theta_{\varepsilon a}=0$; $\sin\theta_{\varepsilon a}=1$) of the outgoing spherical wave. The maximum size of $P_l^1(\cos\theta_{aR})$ is $(l+1)/2$ but all of the partial waves do not reach this maximum for the same angle. Nevertheless we can roughly say that this third term will peak near $\theta_{aR}\sim 20°$, giving a curved-wave correction approximately $r_0/2a$ smaller than the first term.

To recap our assignment of the terms in the differential spherical-wave formula to specific curved-wave corrections, we associate the first term (containing f_{aR}^{00}) with the fundamental, angular-momentum-independent nature of the incident wave, the second term (containing f_{aR}^{10}) with radial corrections dependent on angular momentum, and the third term (containing f_{aR}^{01}) with angular corrections dependent on angular momentum. From this assignment, we can expect significant curved-wave corrections to the single-scattering ARPEFS formula when the following occurs:

(i) the scattering potential is near a node in the incident wave angular distribution;

(ii) the scattering angle is near 0° (forward scattering); or

(iii) the scattering factor is near resonance.

We now consider these cases in more detail.

When the center of a scattering potential lies in a nodal surface of the incident wave, the plane-wave model, Eq.

(11), predicts no scattering. For $l=1$ incident waves, this geometry means $\theta_{\varepsilon a}=90°$ and $\cos\theta_{\varepsilon a}=0°$. Thus only the third term of the differential formula is nonzero and thus this third term represents the entire curved-wave correction for this geometry. It is interesting to note that the usual experimental geometries[6] for ARPEFS prevent this third term from producing its maximum effect. To maximize the measured photocurrent, the electron detector in the direction **R** is usually placed nearly parallel to $\boldsymbol{\varepsilon}$ ($\theta_{\varepsilon R}\sim 0°$). If an atom has $\theta_{\varepsilon a}\sim 90°$ so that $\sin\theta_{\varepsilon a}\sim 1$, then the scattering angle, θ_{aR}, must also be $\sim 90°$ for the scattered wave to enter the detector: for this experimental geometry the condition ($\theta_{\varepsilon a}\sim 90°$, $\theta_{aR}\sim 20°$) will never be satisfied.

Just the opposite must be true for the unusual experimental geometry adopted by Sinkovic *et al.* in a recent azimuthal photoelectron diffraction experiment.[16] They selected $\theta_{\varepsilon R}=72°$ and measured electrons emitted 10° from the surface; many of the important forward scattering atoms would have $\sin\theta_{\varepsilon a}>0.5$, $\cos\phi_{\varepsilon aR}=1$, and $\theta_{aR}\sim 20°$. Thus their observation that plane-wave calculations gave poor agreement with experiment may reflect the neglected variation in wave amplitude across the scattering potential rather than multiple-scattering effects.

When the scattering angle is near 0° we can get large curved-wave corrections strictly from the difference between the first term containing f^{00}_{aR} and the plane-wave limit. To demonstrate this we expand $d_l(ka)$ according to Eq. (23), and subtract the asymptotic plane-wave part:

$$(f^{00}_{aR}-f^{\text{plane}}_{aR})\approx\frac{1}{ik}\sum_{l=0}^{l_{\max}}(2l+1)T_l(k)\left[\frac{l(l+1)}{2ika}\right]\times P_l(\cos\theta_{aR})\ . \tag{35}$$

The maximum difference will occur for forward scattering since $P_l(1)=1$ and all the partial-wave corrections add up. Conversely the minimum curved-wave corrections should be expected for backscattering since $P_l(-1)=(-1)^l$ and successive partial waves tend to cancel. This overall description should be most accurate for higher energies where the partial-wave amplitudes, $T_l(k)$, have little structure.

When the full-scattering factor approaches zero near a generalized Ramsauer-Townsend resonance[17] we can expect the third case for large curved-wave corrections. For special values of electron wave vector, k, and scattering angle, θ_{aR}, the partial-wave sum will be zero due to exact cancellation of all partial-wave components. The particular pair of values (k,θ_{aR}) at which the scattering factor becomes zero will differ between the plane-wave and spherical-wave models as they weight the individual partial waves differently. Thus analysis of scattering resonance data with a plane-wave model will give incorrect scattering angles and the observed resonance energy position will not be correctly given by plane-wave calculations. While the first two circumstances leading curved-wave effects discussed above involve only one or another of the terms in the formula, the resonance calculation will depend in detail on all three terms.

Curved-wave corrections to the EXAFS formula are directly analogous to the corrections for photoelectron diffraction. Since the "detector" for EXAFS is the photoemitting atom, the curved-wave effects are squared: our detector is not asymptotically far from the scattering atom. The first term of the spherical-wave scattering factor

$$\frac{\cos^2\theta_{\varepsilon a}}{ik}\sum_{l=0}^{l_{\max}}(2l+1)T_l(k)(-1)^l\times\left[d_1(ka)d_l(ka)-i\frac{\partial d_l(ka)}{\partial(ka)}\right]^2 \tag{36}$$

has the same angular dependence as the plane-wave model. This term contains both the basic radial correction for $1/ika$—the first factor inside the large parentheses—and the radial derivative correction. As discussed above, the radial derivative factor is usually much smaller than the s-wave origin-shift.

The second term of the EXAFS spherical-wave amplitude factor has the opposite angular dependence compared to a plane-wave model:

$$\frac{\sin^2\theta_{\varepsilon a}}{ik}\sum_{l=0}^{l_{\max}}(2l+1)T_l(k)(-1)^l\left[\frac{d_l(ka)}{ka}\right]^2\frac{l(l+1)}{2}\ . \tag{37}$$

This term corrects for variation in the incident wave amplitude across the potential, primarily due to the node in the p-wave angular distribution. Thus for atoms along the nodal plane perpendicular to the electric vector, this term represents the error made by neglecting the angular structure in the photoelectron wave.

Typically EXAFS analysis is not concerned with relative scattering amplitude of individual atoms. Most of the measurable signal comes from nearest-neighbor atoms, all of which contribute oscillations of the same frequency. The overall EXAFS amplitude is not simply given by the magnitude of the scattering amplitude[18,19] and hence the spherical-wave corrections to the magnitude are of little consequence. Rather it is the phase of the scattering factor that is central to the EXAFS analysis and high precision should require spherical-wave correction; the weight of the individual partial waves in the scattering factor sum will otherwise be incorrect. Of course, practical EXAFS analysis does not rely on the accuracy of the theoretical factor: empirical phase shifts are nearly always derived from known model compounds.

An important EXAFS technique which does rely on relative scattering amplitudes is the polarization dependence employed to determine structures on surfaces.[20] Here the overall amplitude for nearest neighbors is measured for several orientations of the polarization vector with respect to the crystalline sample axis. The results are usually fitted to the angular distribution predicted by a plane-wave model—$\cos^2\theta_{\varepsilon a}$—and ignores spherical-wave effects. We would expect the largest curved-wave correction when ka is small, i.e., low Z elements having short bond lengths and in the lower-energy region, and when we need accurate angular distribution calculations for small $\cos^2\theta_{\varepsilon a}$.

Looking back at the EXAFS formula we also find some

insight into the success of the plane-wave model. The leading correction to the plane-wave amplitude is

$$\Delta = \left[\frac{E_{\rm sph}}{\cos^2\theta_{\varepsilon a}} - f_{\rm aR}^{\rm plane}(\pi) \right] \sim \frac{1}{ik} \sum_{l=0}^{l_{\max}} (2l+1) T_l(k) (-1)^l \frac{l(l+1)}{ika} . \quad (38)$$

This term is just twice the correction for backscattering ARPEFS, and, as we argued above, the successive terms tend to cancel.

IV. CURVED-WAVE CORRECTIONS TO THE SCATTERING FROM Ni ATOMS

Now we turn to some specific examples of curved-wave effects in the scattering of electrons from Ni atoms. We will begin by examining the angle dependence of the scattering factors at 5 Å^{-1} (95 eV) and at 10 Å^{-1} (381 eV), followed by their k and r dependences. For each case we will compare $f_{\rm aR}^{00}$ to the plane-wave limit, $f_{\rm aR}$. As the last example we calculate the effect of curved-wave corrections to the polarization dependence in surface EXAFS. In all these examples we take $|\mathbf{a}| = 2.23$ Å.

Figure 1 compares the amplitudes of $f_{\rm aR}^{00}$ and $f_{\rm aR}$ for scattering angles from 0° to 180° at a wave number of 5 Å^{-1} [see Eq. (28)]. The general trend confirms our qualitative discussion in the preceding section: the largest corrections are in the forward-scattering directions. Figure 2 gives the amplitude of $f_{\rm aR}^{10}$ [Eq. (29)]; note the dramatic reduction in magnitude. The angular structure of $f_{\rm aR}^{10}$ is rather similar to $f_{\rm aR}^{00}$.

The angular spherical wave correction, Eq. (31), is plotted in Fig. 3 as $|\sin\theta_{\rm aR} f_{\rm aR}^{01}|$ to emphasize the fact that this correction is zero for forward ($\theta_{\rm aR}=0°$) and exactly backscattering ($\theta_{\rm aR}=180°$). The overall scale is 20% of the scale in Fig. 7, but recall that two additional angle factors, $\sin\theta_{\varepsilon a}$ and $\cos\phi_{\varepsilon a R}$, reduce this correction unless the scattering geometry is special.

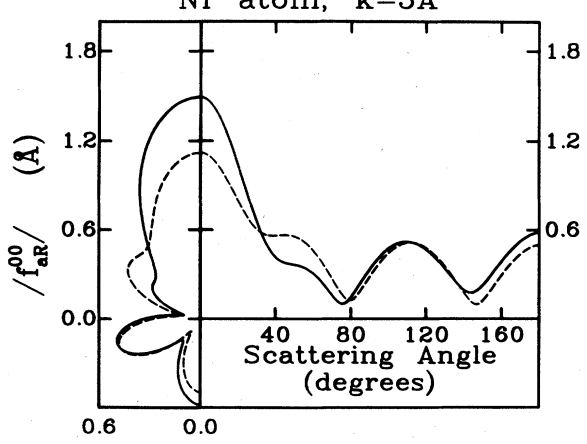

FIG. 1. Scattering factor amplitude in Å for Ni atom potential at $k=5$ Å^{-1} (95 eV). Solid line is $|f_{\rm aR}^{00}|$, the $l=0$ spherical-wave scattering factor; dashed line, plane-wave limit $2ka \gg l(l+1)$. Right-hand panel gives Cartesian plots of factor magnitude versus scattering angle, $\theta_{\rm aR}$ in degrees; left-hand panel is a polar plot with $\theta_{\rm aR}=0°$ running up the figure.

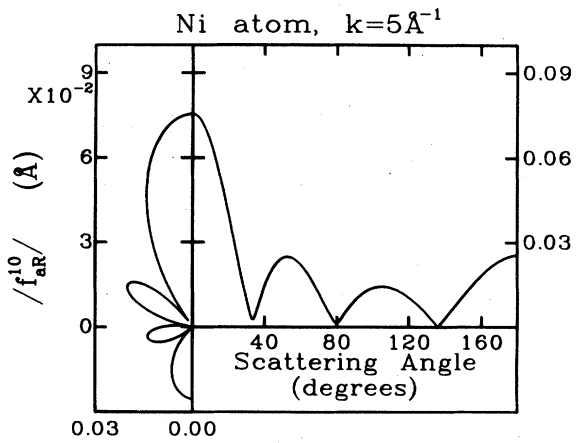

FIG. 2. Radial derivative scattering factor amplitude, $|f_{\rm aR}^{10}|$ in Å for Ni atom potential at $k=5$ Å^{-1} (95 eV). Format described in Fig. 1. Note the scale of this figure is $\frac{1}{20}$th of Fig. 1.

We have constructed Figs. 4, 5, and 6 to parallel Figs. 1, 2, and 3, respectively, except $k=10$ Å^{-1} for these new figures. All three comparisons demonstrate that the curved-wave corrections are not much smaller at this higher energy, but the cancellation of successive angular momenta due to $P_l(\cos\theta) \approx (-1)^l$ is much more effective. Thus all the large scattering angle ($\theta > 90°$) amplitudes are quite accurate (5%) in the plane-wave model, while the amplitude for scattering through 32° is too high by more than a factor of 2.

We can also compare the scattering factor phase by plotting the argument of the complex ratio $f_{\rm aR}^{00}/f_{\rm aR}$, i.e., their phase difference, as in Fig. 7. For $k=5$ Å^{-1}, the phase difference is roughly $+0.5$ rad; note that the two angles where the phase difference is not near $+0.5$

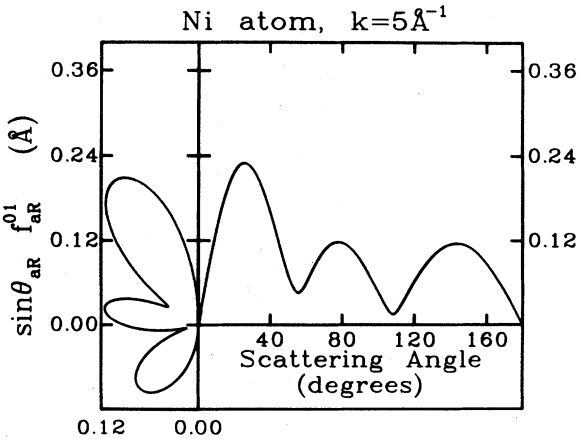

FIG. 3. Angular derivative scattering factor amplitude $|f_{\rm aR}^{01}|$ times sine of the scattering angle, $\theta_{\rm aR}$, in Å for Ni potential at $k=5$ Å^{-1} (95 eV). Format described in Fig. 1. This scattering factor cannot contribute in near forward or near backscattering directions.

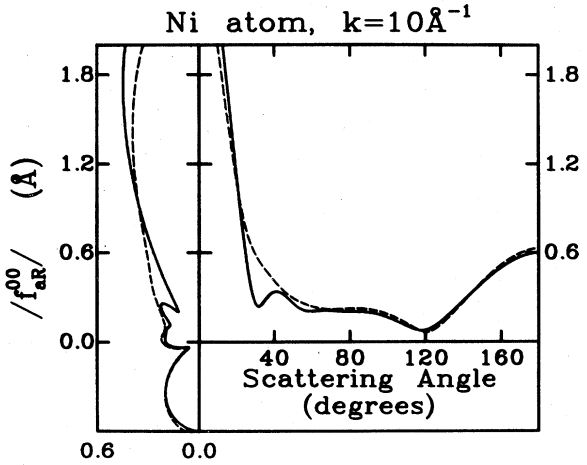

FIG. 4. Identical to Fig. 1, except $k=10$ Å^{-1} (381 eV). Note the improved accuracy of the plane-wave limit for backscattering angles. The figure has the same scale as Fig. 1 to emphasize backscattering angles.

rad correspond to scattering angles with small scattering amplitudes, see Fig. 1. The curve for $k=10$ Å^{-1} has the same behavior although the shift is about half as large.

The k dependence of these scattering factors is illustrated for $\theta_{aR}=173°$ in Fig. 8, $\theta_{aR}=0°$ in Fig. 9, and $\theta_{aR}=127°$ in Fig. 10. The backscattering geometry, Fig. 8, is the most important one for ARPEFS and, fortunately, the plane-wave model is rather accurate. As we noted above, the angular curved-wave correction is eliminated by $\sin\theta_{aR}\sim 0$ for backscattering, and Fig. 8 shows that f^{10}_{aR} is very much smaller than f^{00}_{aR}. Thus f^{00}_{aR} by itself characterizes the backscattering of $l=1$ waves. Notice also that the plane-wave amplitude error approaches a constant not equal to zero, for large k. This is explained in the same manner as the EXAFS discussion in the preceding section.

The greatest curved-wave corrections occur in the forward directions; Fig. 9 gives the example of $\theta_{aR}=0°$. The plane-wave amplitude is roughly 0.2 Å too small over the entire range in k. Without the alternating sign of

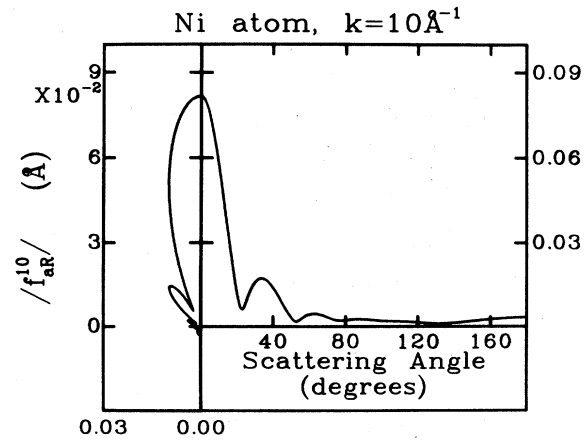

FIG. 5. Identical to Fig. 2 except for $k=10$ Å^{-1} (381 eV).

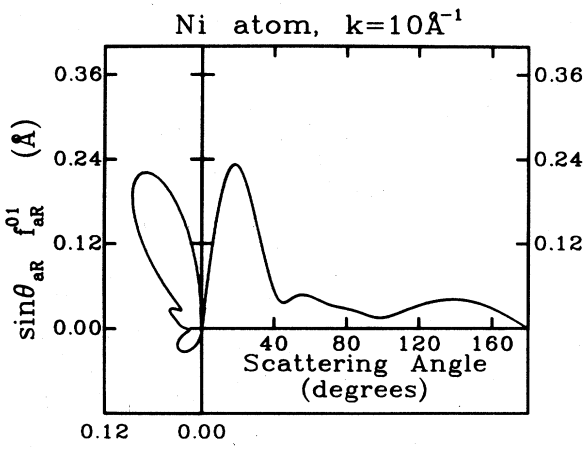

FIG. 6. Identical to Fig. 3, except for $k=10$ Å^{-1} (381 eV). Note that shift of the main peak to lower angles; its amplitude is similar to the amplitude of the main peak at $k=5$ Å^{-1}, but the correction for backscattering is very much smaller now.

$P_l(-1)$ characteristic of backscattering, we see no approach to the plane-wave limit at large k. Again f^{10}_{aR} is very small, at least a factor of 20 below f^{00}_{aR}; f^{01}_{aR} cannot contribute to forward scattering as long as $\theta_{aR}<\sim 10°$. The phase difference (not plotted) between f^{00}_{aR} and f^{plane}_{aR} is ~ 0.7 rad.

Finally, we consider scattering through 127°, the position of a generalized Ramsauer-Townsend resonance in Ni. The resonance is a crossing of the origin in the complex plane by the complete scattering factor. The resonance position in energy and angle depends crucially on the cancellation of many partial waves and hence cannot be correctly predicted with a plane-wave calculation. Figure 10 displays the scattering factors for $\theta_{aR}=127°$. The factors $|f^{00}_{aR}|$ and $|f^{plane}_{aR}|$ are reasonably close except in the resonance region near 8 Å^{-1}. The angular curved-wave correction is now significant, especially since it conspires with f^{00}_{aR} to make the overall scattering amplitude

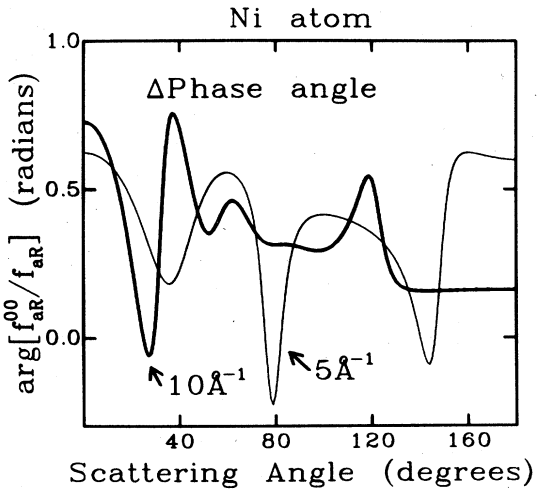

FIG. 7. Difference in phase (in rad) between spherical and plane-wave models versus scattering angle θ_{aR} in degrees, for scattering from Ni atom potentials at $k=5$ Å^{-1}.

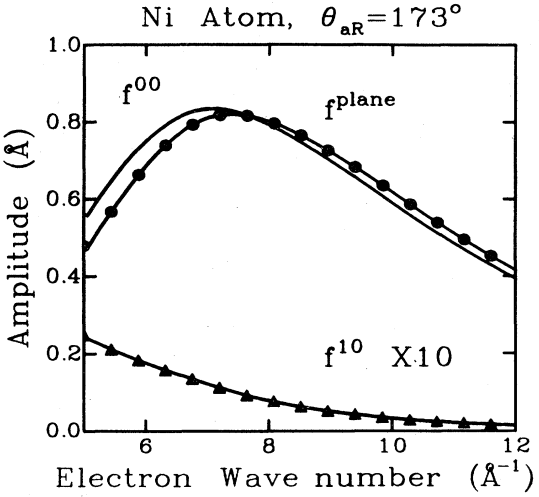

FIG. 8. Scattering factor amplitudes in Å versus electron wave number ($Å^{-1}$) for near backscattering ($\theta_{aR}=173°$) from Ni atom potentials. Solid-line, basic spherical scattering factor f^{00}_{aR}; circles, plane-wave limit scattering factor f_{aR}; triangles, radial derivative scattering factor f^{10}_{aR}. The plane-wave factor is rather close to the spherical wave f^{00}_{aR} and the other spherical-wave corrections are very small at all energies; notice also that plane-wave error approaches a nonzero constant.

zero at $k=7.5$ $Å^{-1}$. (f^{10}_{aR} has not been plotted; it is very small for $\theta_{aR}=127°$.) The difference between exact single-scattering and plane-wave calculations is more dramatic in the phase of the scattering factor. Calculations done for values of ka corresponding to recent experimental measurements[17] are shown in Fig. 11. The phase jump at resonance is not correctly placed in angle or energy in the plane-wave limit.

To estimate the distance $|\mathbf{a}|$ beyond which we can

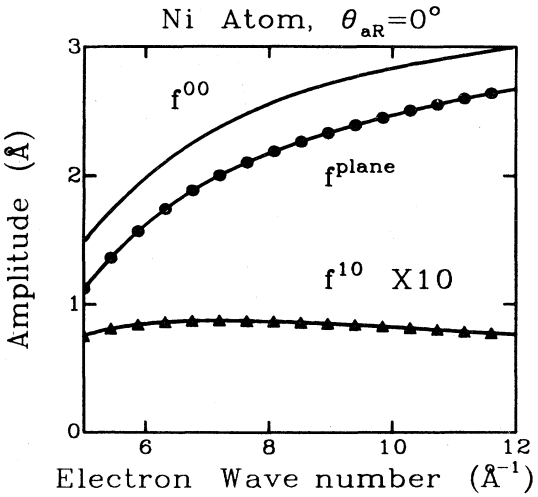

FIG. 9. Scattering factor amplitude in Å versus electron wave number ($Å^{-1}$) for forward scattering ($\theta_{aR}=0°$). Solid line, basic spherical scattering factor f^{00}_{aR}; circles, plane-wave limit scattering factor f_{aR}; triangles, radial derivative scattering factor f^{10}_{aR}. Note the nearly constant plane-wave error; the radial derivative correction becomes almost 10% at low energies.

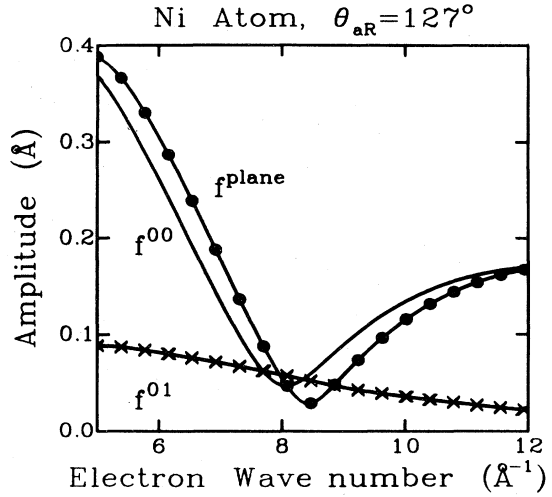

FIG. 10. Scattering factor amplitudes in Å versus electron wave number ($Å^{-1}$) for scattering through $\theta_{aR}=127°$, the position of a generalized Ramsauer-Townsend resonance. Solid line, basic spherical-wave factor f^{00}_{aR}; circles, plane-wave limit f^{plane}_{aR}; crosses, angular derivative f^{01}_{aR}. The radial derivative is negligible at this angle for all energies.

safely use the plane-wave formula, we plot in Fig. 12 the radius at which $|f^{00}_{aR}-f^{plane}_{aR}|\leq 0.06$ Å, for two energies, $k=5$ $Å^{-1}$ and $k=10$ $Å^{-1}$. This criterion for the allowable error in scattering factor was chosen to be $\sim 10\%$ of the backscattering ($\theta_{aR}=180°$) amplitude for Ni. We see from this figure that plane-wave calculations are never adequate by this criterion for forward scattering at any energy or any practical radius. For angles greater than 45°, most scattering atoms within 10 Å of the photoemitter would require curved-wave corrections in the lower-energy region, while perhaps only the nearest neigh-

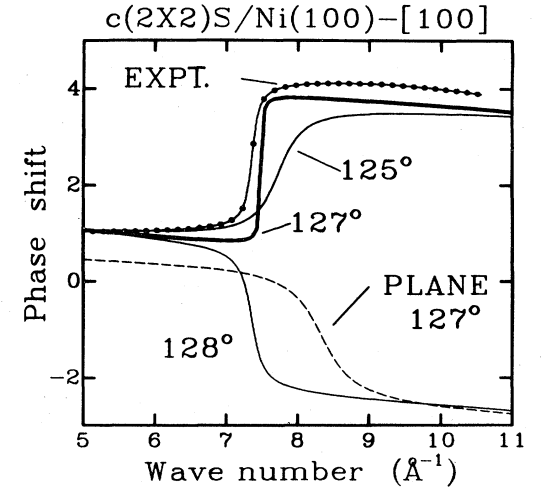

FIG. 11. Phase shifts for scattering from Ni. The dashed line shows the phase-shift function ϕ_j calculated with plane-wave theory for $\theta=127°$. The dotted line is the phase shift from the experimental curve. The zero crossing jump in phase occurs too high in wave number in the plane-wave limit. Solid lines are curved-wave calculations of the phase shift function for the indicated scattering angles.

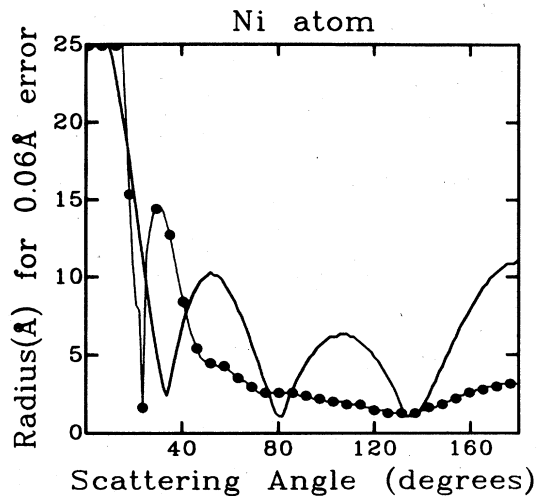

FIG. 12. Radius for acceptable results from plane-wave calculations versus bond angle for $k=5$ Å^{-1} (solid line) and $k=10$ Å^{-1} (line with circles). The radii were selected so that all distances greater than the plotted lines have $|f^{00}_{aR}-f^{plane}_{aR}|<0.06$ Å.

bors require these extra calculations for $k=10$ Å^{-1}.

To discuss an example calculation for the curved-wave EXAFS formula, we adopt the second form for $\chi(k)$ given in Appendix B, Eq. (B13). Figure 13 compares f^{iso} to its asymptotic limit $f^{plane}_{aR}(\pi)$ and to f^{an}. We see a close analogy between f^{iso} for EXAFS and f^{00}_{aR} for ARPEFS, but the curved-wave corrections are larger for EXAFS (compare Fig. 8) since the "detector" is not asymptotically far from the scattering atom. Once again the large k region approaches a nonzero constant plane-wave error. Perhaps most interesting, $|f^{an}|$ is seen to be nearly 2 orders of magnitude smaller than $|f^{iso}|$ in this energy range. Thus, at least for Ni atoms, the standard EXAFS formula with f^{iso} replacing $f^{plane}_{aR}(\pi)$ would give 1% accurate curved-wave results. Furthermore, since the polarization dependence technique relies only on the assumption that the oscillations are proportional to $\cos^2\theta_{\varepsilon a}$, curved-wave corrections to the calculated amplitude ratios are entirely insignificant.

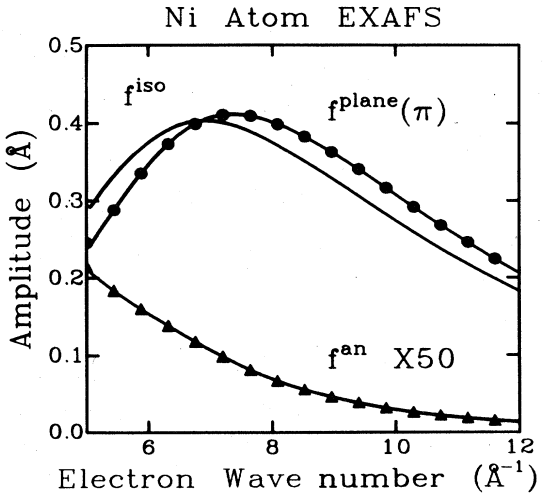

FIG. 13. Scattering factors for (1s) EXAFS. Solid line is f^{iso}, the curved-wave scattering amplitude defined by Eq. (B11). Line with circles is the plane-wave limit which has a similar shape to f^{iso}. Line with triangles is f^{an}, Eq. (B12) multiplied by a factor of 50.

V. DISCUSSION

We have derived new formulas and given examples for the curved-wave scattering of $l=1$ spherical waves. What can we expect for more general spherical waves? We offer some qualitative ideas in this section.

We envision two important cases: (i) photoabsorption by p, d, and f core levels giving spherical waves with higher angular momenta and magnetic sublevel occupations; and (ii) multiple scattering preceded either by photoelectron scattering or plane-wave scattering typical for the LEED experiment. Both of these problems can be approached by the method we use here for $l=1$ waves. That is, the origin-shift addition theorem summed over magnetic sublevels can be differentiated to higher and higher order. The resulting expressions will be formidable so we will be content with estimates for now.

First we consider higher l waves populated by photoemission. For core orbital initial states with p, d, or f orbital angular momentum, two partial waves with $l\pm1$ will be created. Each partial wave may be treated by the method of Sec. II. We should always get a first term such as $d_l(ka)Y_{lm}(a)f^{00}_{aR}$, the amplitude of the l spherical wave times the scattering factor for $l=0$ waves. This is the only curved-wave factor which survives the asymptotic limit and hence will always be the most important. Our discussion for $l=1$ virtually ignores $d_l(ka)$ as being close to 1.0, but for higher angular momenta this factor may be important. Otherwise, this first term will follow the trends discussed in the preceding section.

We should also always get curved-wave corrections due to differences between the $(1/ikr)$ dependence of $h_0(kr)$ and the angular-momentum-dependent radial wave character through the potential region—corrections analogous to f^{10}_{aR}. For higher angular momenta, the difference between the radial character of the incident spherical wave and the radial character of $h_0(ka)$ already included in the first term will increase. We might conclude from our Ni example calculations that these radial variations are negligible for $l=1$ waves; for some higher l we will be forced to include this term.

For all l, the radial variations should be less than the angular variations simply because spherical waves (except $l=0$) have stronger angle dependence. Thus curved-wave corrections analogous to f^{01}_{aR} will be increasingly important for higher angular momenta. These angular corrections are always greatest near nodes in the incoming wave, where the wave amplitude is changing most rapidly. The nodal regions have the least amplitude and the finite extent of the potential is averaging opposite phase waves across the nodal surface, smoothing out the nodal structure. Hence, on the average, even these angular corrections will not be large. The phrase "on the average" is connected with the additional angular vectors such as $\sin\theta_{\varepsilon a}\sin\theta_{aR}\cos\phi_{\varepsilon aR}$ which multiply the curved-wave angular correction.

In addition to more significant curved-wave corrections

of the same type as the $l=1$ wave, higher angular momenta waves should also have corrections corresponding to higher-order derivatives. Thus the second derivatives of the incoming wave across the extent of the potential will become important for some high l. Actual calculations are necessary to determine how important these corrections will be.

This leads us to the second important case, multiple scattering. While photoabsorption can populate only dipole-allowed angular momenta, an outgoing scattered wave contains all angular momenta up to $l_{\max} \sim kr_0$. To apply the method of this paper to the exact multiple scattering of spherical waves would—as a practical matter—require automation of the derivative calculations, a dubious improvement over the Gaunt-integral summation formula, Eq. (12). On the other hand, the outgoing scattered wave is no more than a spherical wave with an angular dependence and phase determined by scattering rather than by photoabsorption. Thus, approximate multiple scattering could be calculated by starting with f_{aR}^{00} times the single-scattered wave amplitude at the second scattering center and adding curved-wave corrections by numerical differentiation of the single-scattered wave function.

VI. CONCLUSION

To summarize our work we have accomplished the following:

(i) derived new curved-wave formulas for single scattering of $(1s)$ core-level photoelectrons, appropriate for ARPEFS and EXAFS experiments;

(ii) interpreted the individual scattering factors in this formula as different types of curved-wave corrections, allowing some guidelines to be devised to predict which scattering problems require curved-wave formulas;

(iii) given some idea of the size of these factors for Ni atom scattering; and

(iv) discussed the possible generalization to higher angular momenta core levels.

The significance of these results is partly formal and partly practical. The remarkable accuracy of the plane-wave model has been widely recognized,[4,21] but often attributed to the asymptotic limit of the spherical wave. Our new formulas more clearly demonstrate the origin of this convenience: the improved cancellation of partial waves at large k. Thus the accuracy of the plane-wave model does not improve for large k in forward scattering directions. This point may also be made by a semiclassical argument. As Fig. 14 illustrates, forward scattering corresponds to large classical impact parameters;[22] backscattering corresponds to low impact parameters that orbit the strong attractive center region of the potential. The wave-front curvature corrections are thus much larger for forward scattering directions which sample the extreme edges of the potential.

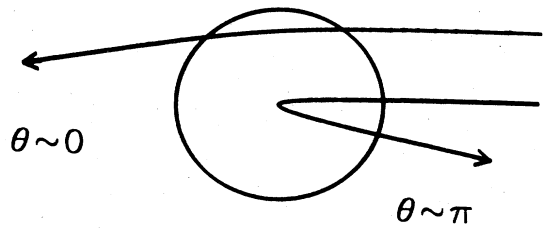

FIG. 14. Schematic semiclassical orbits for an attractive potential. If the circle represents the effective radius of a screened nuclear charge, then particles with large impact parameters will sample only the weak outer region of the potential and scatter through small (forward) angles. Particles with small impact parameters orbit the strong nuclear attraction and exit at large (backscattering) angles. The connection to wave scattering is made through $b=l/k$ where b is the impact parameter: large l partial waves contribute to forward scattering and small l waves dominate for backscattering.

On the practical side, our new curved-wave formulas are scarcely more complicated than the plane-wave versions. Some advantage may also be made of the different angle dependences of each scattering factor, to minimize numerical computations. Hopefully, our qualitative discussion and numerical example will serve as some guide to estimate when curved-wave effects may be important. Finally, we have demonstrated that curved-wave EXAFS calculations can be quite accurate with only a minor modification of the plane-wave formula, a result which extends the recent work of Schaich[23] and of Gurman *et al.*[24]

Unfortunately, it is also clear from our results that curved-wave effects cannot explain the difference between ARPEFS experiments and the single-scattering plane-wave calculations of Bullock, Fadley, and Orders.[7] The curved-wave corrections are typically $\sim 20\%$ and only that large in the forward directions. Thus while we have reduced the computational barrier to using curved-wave calculation for ARPEFS, we can also conclude that the major discrepancies between theory and experiment are not due to curved-wave corrections at least for single backscattering.

We can characterize the disagreement between model calculations and ARPEFS measurements by noting that scatterings from nearest neighbors and backscatterings from non-nearest neighbors appear to be much more dominant than predicted theoretically. Wave-front curvature increases scattering for some angles, decreases it for others, and generally has less effect for backscattering. Therefore, while curved-wave formulas may be important for accurate calculation, there are larger errors elsewhere in the theory. Multiple scattering must be part of the answer: as Fig. 4 illustrates, forward scattering is large in the ARPEFS energy range and should not be neglected. Our results here predict that this forward scattering cannot be calculated within the plane-wave formulation. There may also be errors in the inelastic scattering and thermal averaging. We must investigate these questions in further work.

ACKNOWLEDGMENTS

This work was supported by the Director, Office of Energy Research, Office of Basic Energy Sciences, Division of Chemical Sciences, U. S. Department of Energy under Contract No. DE-AC03-76SF00098.

APPENDIX A: ALTERNATE DERIVATION FOR DIFFERENTIAL FORM OF ORIGIN-SHIFT ADDITION THEOREM

We may arrive at the results of Sec. II by an entirely different route. We will use a series of well-known formulas conveniently tabulated in Pendry,[1] his Appendix A.

We begin with the origin-shift addition theorem for $(l,m)=(1,0)$, Eq. (12). Using the definition of Y_{10} and the recursion relation for Y_{lm}, we find

$$G_{10,l'',m''}=4\pi\sum_{l',m'}\left\{i^{l'}h_{l'}(ka)Y^*_{l'm'}(\hat{\mathbf{a}})\left[\left[\frac{3}{4\pi}\right]^{1/2}A^0_{l''+1,-m''}\int Y_{l'm'}(\hat{\mathbf{K}})Y^*_{l''+1,m''}(\hat{\mathbf{K}})d\Omega_{\mathbf{K}}\right.\right.$$
$$\left.\left.+\left[\frac{3}{4\pi}\right]^{1/2}A^0_{l'',-m''}\int Y_{l'm'}(\hat{\mathbf{K}})Y^*_{l''-1,m''}(\hat{\mathbf{K}})d\Omega_{\mathbf{K}}\right]\right\}. \tag{A1}$$

In other words, since Y_{10} is proportional to $\cos(\theta)$, the product $Y_{10}Y^*_{l''m''}$ becomes the recursion relation for $Y_{l''m''}$. The factor

$$A^0_{lm}=\left[\frac{(l+m)(l-m)}{(2l+1)(2l-1)}\right]^{1/2} \tag{A2}$$

is related to the ratios of the normalizing coefficients of spherical harmonics. The remaining integrals in $G_{10,l''m''}$ are the orthonormality conditions for spherical harmonics:

$$\int Y_{l'm'}(\hat{\mathbf{K}})Y_{l''+1,m''}(\hat{\mathbf{K}})d\Omega_{\mathbf{K}}=\delta_{l',l''+1}\delta_{m'm''} \tag{A3}$$

and the sum on l',m' simplifies to

$$G_{10,l''m''}=\left[\frac{3}{4\pi}\right]^{1/2}4\pi[A^0_{l+1,-m''}i^{l''+1}h_{l''+1}(ka)Y^*_{l''+1,m''}(\hat{\mathbf{a}})+A^0_{l'',-m''}i^{l''-1}h_{l''-1}(ka)Y^*_{l''-1,m''}(\hat{\mathbf{a}})]\,. \tag{A4}$$

The factor inside the square brackets is the result of a differential operation on $i^{l''}h_{l''}(ka)Y^*_{l'',m''}$. Rewriting Nozawa's[12] Eq. (3.8) in terms of normalized spherical harmonics shows that

$$\left[\frac{-i}{k}\frac{\partial}{\partial z}\right]i^{l''}h_{l''}(ka)Y^*_{l''m''}(\hat{\mathbf{a}})=[A^0_{l''+1,-m''}i^{l+1}h_{l''+1}(ka)Y^*_{l''+1,m''}(\hat{\mathbf{a}})+A^0_{l'',-m''}i^{l''-1}h_{l''-1}(ka)Y^*_{l''-1,m''}(\hat{\mathbf{a}})]\,. \tag{A5}$$

Thus

$$G_{10l''m''}=\left[\frac{3}{4\pi}\right]^{1/2}4\pi\left[-\frac{i}{k}\frac{\partial}{\partial z}\right]i^{l''}h_{l''}(ka)Y^*_{l''m''}(\hat{\mathbf{a}}) \tag{A6}$$

with

$$\frac{1}{k}\frac{\partial}{\partial z}=\cos\theta_{\varepsilon\mathbf{a}}\frac{1}{k}\frac{\partial}{\partial a}-\frac{\sin\theta_{\varepsilon\mathbf{a}}}{ka}\frac{\partial}{\partial\theta_{\varepsilon\mathbf{a}}}$$
$$=\cos\theta_{\varepsilon\mathbf{a}}\frac{1}{k}\frac{\partial}{\partial a}-\frac{\cos\theta_{\varepsilon\mathbf{R}}-\cos\theta_{\varepsilon\mathbf{a}}\cos\theta_{\mathbf{aR}}}{ka}\frac{\partial}{\partial(\cos\theta_{\mathbf{aR}})}\,. \tag{A7}$$

The addition theorem for spherical harmonics then leads to the results in Eq. (19). We can avoid the derivative operation altogether by applying the recursion formulas for $h_{l''}$ and $Y_{l''m''}$, but this approach is tedious.

APPENDIX B: APPLICATION TO EXAFS

We apply the approach of Sec. II to the spherical-wave single-scattering extended x-ray absorption fine structure. Schaich[23] and Gurman *et al.*[24] recently derived simplified, exact EXAFS formulas for cubic or polycrystalline environments. Here we consider only $(1s)$ core-level excitation and linearly polarized light, but we allow a general environment. With the $\hat{\mathbf{z}}$ axis along the polarization vector, the dipole selection rules reduce Schaich's Eq. (3) for the x-ray-absorption coefficient to

$$\mu_c=A_4\mathrm{Im}[M^2_{01}(i+\chi_1)]\,. \tag{B1}$$

Our $(i+\chi_1)$ corresponds to Schaich's χ_{11}. We are interested only in the oscillations, χ_1; we refer to Schaich for the radial matrix elements M_{01} and constants in A_4. Transcribing Schaich's Eq. (5) into our notation gives

$$\chi_1(k)=\sum_{\mathbf{a}\,(\neq 0)}\sum_{l'',m''}[e^{i\delta'_1}(i)G_{l''m''10}(-k\mathbf{a})(-i)$$
$$\times T_{l''}(k)G_{10l''m''}(k\mathbf{a})(-i)e^{i\delta'_1}]\,. \tag{B2}$$

The factor $e^{i\delta'_1}$ is the absorber atom phase shift which cancels in the photoelectron diffraction experiment and hence was dropped from the formulas of Sec. II.

To apply the differential form from Appendix A, note that

$$G_{l''m''10}(-k\mathbf{a})=(-1)^{m''}G_{10l'',-m''}(-k\mathbf{a})\,. \tag{B3}$$

This is a consequence of the conjugation property of spherical harmonics.

With the differential forms for the origin-shift addition theorem coefficients, we have

$$\chi_1(k)=\sum_{\hat{\mathbf{a}}\,(\neq 0)}\left\{3e^{2i\delta_1'}\sum_{l''}\left[\left[\frac{1}{ik}\frac{\partial}{\partial z'}\right]\left[\frac{1}{ik}\frac{\partial}{\partial z}\right]\sum_{m''}[4\pi i^{l''}h_{l''}(ka')Y_{l''m''}(\hat{\mathbf{a}}')(-i)T_{l''}(k)i^{l''}h_{l''}(ka)Y^*_{l''m''}(\hat{\mathbf{a}})]\right]\right\}. \tag{B4}$$

The primes distinguish outgoing and backscattered waves until the derivatives are complete. The addition theorem for spherical harmonics simplifies this expression, and we employ our separation of spherical waves into asymptotic and polynomial parts to write

$$\chi_1(k)=-\sum_{\mathbf{a}\,(\neq 0)}\left\{3e^{2i\delta_1'}\sum_{l''}\left[(2l+1)\left[\frac{1}{ik}\frac{\partial}{\partial z'}\right]h_0(ka')d_{l''}(ka')\left[\frac{1}{ik}\frac{\partial}{\partial z}\right]h_0(ka)d_l(ka)P_{l''}(\cos\theta_{\mathbf{aa}'})\right]\right\}, \tag{B5}$$

where $\cos\theta_{\mathbf{aa}'}$ will ultimately be -1. The first derivative becomes

$$\left[\frac{1}{ik}\frac{\partial}{\partial z}\right]h_0(ka)d_{l''}(ka)P_{l''}(\cos\theta_{\mathbf{aa}'})=h_0(ka)\left[d_1(ka)d_{l''}(ka)\cos\theta_{\varepsilon\mathbf{a}}P_{l''}(\cos\theta_{\mathbf{aa}'})+\frac{\cos\theta_{\varepsilon a}}{ik}\frac{\partial d_{l''}(ka)}{\partial(a)}P_{l''}(\cos\theta_{\mathbf{aa}'})\right.$$
$$\left.+\frac{(\cos\theta_{\varepsilon\mathbf{a}'}-\cos\theta_{\varepsilon\mathbf{a}}\cos\theta_{\mathbf{aa}'})}{ika}d_{l''}(ka)\frac{\partial P_l(\cos\theta_{\mathbf{aa}'})}{\partial(\cos\theta_{\mathbf{aa}'})}\right]. \tag{B6}$$

The first term in this expression is a consequence of the derivative as a lifting operator. After the second derivative we may set $a'=a$, $P_l(\cos\theta_{\mathbf{aa}'})=(-1)^l$, and $\cos\theta_{\varepsilon\mathbf{a}'}-\cos\theta_{\varepsilon\mathbf{a}}\cos\theta_{\mathbf{aa}'}=0$. We also need the value of $dP_l(x)/dx$ for $x=(-1)$; it is equal to $(-1)^{l+1}l(l+1)/2$. Thus we have

$$\chi_1(k)=-\sum_{\mathbf{a}\,(\neq 0)}\left[3e^{2i\delta_1'}\frac{e^{2ika}}{ka^2}\frac{1}{ik}\sum_{l=0}^{l_{\max}}\left\{(2l+1)T_l(k)(-1)^l\left[\cos^2\theta_{\varepsilon\mathbf{a}}\left[d_1(ka)d_l(ka)-i\frac{\partial d_l(ka)}{\partial(ka)}\right]^2\right.\right.\right.$$
$$\left.\left.\left.-\frac{\sin^2\theta_{\varepsilon\mathbf{a}}}{(ka)^2}[d_l(ka)]^2\frac{l(l+1)}{2}\right]\right\}\right]. \tag{B7}$$

This form most clearly displays the origin of the curved-wave corrections, but to compare to the work of Schaich, note that

$$\frac{1}{ik}\frac{\partial d_l(ka)}{\partial(a)}=d_{l-1}(ka)-d_l(ka)-\frac{l}{ika}d_l(ka) \tag{B8}$$

which—together with the recursion relation for $d_l(ka)$—shows that

$$d_1(ka)d_l(ka)+\frac{1}{ik}\frac{\partial d_l(ka)}{\partial(a)}=\frac{l+1}{2l+1}d_{l+1}+\frac{l}{2l+1}d_{l-1}. \tag{B9}$$

The square of this factor may be reduced with the help of the square of the recursion relation for d_l to give

$$\left[\frac{l+1}{2l+1}d_{l+1}+\frac{l}{2l+1}d_{l-1}\right]^2$$
$$=\frac{l+1}{2l+1}d_{l+1}^2+\frac{l}{2l+1}d_{l-1}^2+\frac{l(l+1)}{(ka)^2}d_l^2. \tag{B10}$$

Then we can define

$$f^{\mathrm{iso}}(\pi)=\frac{1}{ik}\sum_{l=0}^{l_{\max}}\left[(2l+1)T_l(k)(-1)^l\times\left[\frac{l+1}{2l+1}d_{l+1}^2+\frac{l}{2l+1}d_{l-1}^2\right]\right] \tag{B11}$$

and

$$f^{\mathrm{an}}(\pi)=\frac{1}{ik}\sum_{l=0}^{l_{\max}}\left[(2l+1)T_l(k)(-1)^l\frac{l(l+1)}{(ka)^2}d_l^2(ka)\right] \tag{B12}$$

to write

$$\chi(k)=\mathrm{Im}\left[-\sum_{\mathbf{a}\,(\neq 0)}3\frac{e^{2ika}}{ka^2}e^{2i\delta_1'}\left[(f^{\mathrm{iso}}+f^{\mathrm{an}})\cos^2\theta_{\varepsilon\mathbf{a}}-\frac{f^{\mathrm{an}}}{2}\sin^2\theta_{\varepsilon\mathbf{a}}\right]\right]. \tag{B13}$$

In an isotropic or cubic environment, $2\cos^2\theta_{\varepsilon\mathbf{a}}=\sin^2\theta_{\varepsilon\mathbf{a}}$ and the anisotropic scattering factor cancels out to give the same formula derived by Schaich[23] and by Gurman *et al.*[24] Notice that our result demonstrates that the simplification achieved by these authors is not a consequence of symmetry—the general formula is scarcely more complicated than the high symmetry version—but rather is a result of summing over the equivalent magnetic sublevels of the scattered wave.

[1]J. B. Pendry, *Low Energy Electron Diffraction* (Academic, London, 1974).

[2]M. A. Van Hove and S. Y. Tong, *Surface Crystallography by LEED* (Springer, Berlin, 1979).

[3]C. B. Duke, Adv. Chem. Phys. **27**, 1 (1974).

[4]P. A. Lee, P. H. Citrin, P. Eisenberger, and B. M. Kincaid, Rev. Mod. Phys. **53**, 769 (1981).

[5]P. A. Lee, Phys. Rev. B **13**, 5261 (1976).

[6]J. J. Barton, C. C. Bahr, Z. Hussain, S. W. Robey, J. G. Tobin, L. E. Klebanoff, and D. A. Shirley, Phys. Rev. Lett. **51**, 272 (1983).

[7]E. L. Bullock, C. S. Fadley, and P. J. Orders, Phys. Rev. B **28**, 4867 (1983).

[8]*Handbook of Mathematical Functions,* edited by M. Abramowitz and I. A. Stegun, Natl. Bur. Stand. (U.S.) Applied Mathematics Series No. 55 (U.S. GPO, Washington, D.C., 1964).

[9]L. I. Schiff, *Quantum Mechanics,* 3rd ed. (McGraw-Hill, New York, 1968).

[10]P. A. Lee and J. B. Pendry, Phys. Rev. B **11**, 2795 (1975).

[11]This is the same formula as given in Pendry, Ref. 1, his Appendix A, except that factors of i^l have been associated with corresponding spherical Bessel functions. Note that his factor $i^{l-l'-l''}$ is equal to $i^{-l+l'+l''}$ whenever the Gaunt integral is nonzero.

[12]R. Nozawa, J. Math. Phys. **7**, 1841 (1966).

[13]B. Van der Pol, Physica (Utrecht) **3**, 393 (1936).

[14]When the differential operator is applied to generate the addition theorem, derivatives may be taken with either **a** or **r**′ constant, where $\mathbf{a}+\mathbf{r}'=\mathbf{r}$. Nozawa uses the physically more appealing choice of **a** constant; our results follow most readily if **r**′ is constant for the purpose of the lifting operation. The equivalence of these two avenues may be proven by, for example, considering the Fourier-transform derivation of the addition theorem as given by Nozawa.

[15]C. Cohen-Tannoudji, B. Diu, and F. Laloë, *Quantum Mechanics* (Wiley, New York, 1977).

[16]B. Sinkovic, P. J. Orders, C. S. Fadley, R. Trehan, Z. Hussain, and J. Lecante, Phys. Rev. B **30**, 1830 (1984).

[17]J. J. Barton, C. C. Bahr, Z. Hussain, S. W. Robey, L. E. Klebanoff, and D. A. Shirley, Soc. Photo-Optical Instrum. Eng. **447**, 82 (1984); J. J. Barton and D. A. Shirley, Lawrence Berkeley Laboratory Report No. LBL-19325 (unpublished).

[18]J. J. Rehr, E. A. Stern, R. L. Martin, and E. R. Davidson, Phys. Rev. B **17**, 560 (1978).

[19]P. Eisenberger and B. Lengeler, Phys. Rev. B **22**, 3551 (1980).

[20]P. H. Citrin, P. Eisenberger, and R. C. Hewitt, Phys. Rev. Lett. **45**, 1948 (1980).

[21]B. K. Teo, *Proceedings of the International Conference on EXAFS and Near Edge Structure,* edited by A. Bianconi, L. Incoccia, and S. Stipcich (Springer, Berlin, 1983), p. 11.

[22]H. A. Bethe and R. Jackiw, *Intermediate Quantum Mechanics,* 2nd ed. (Benjamin, Reading, MA, 1968).

[23]W. L. Schaich, Phys. Rev. B **29**, 6513 (1984); J. E. Müller and W. L. Schaich, *ibid.* **27**, 6489 (1983).

[24]S. J. Gurman, N. Binsted, and I. Ross, J. Phys. C **17**, 143 (1984).